JOURNAL OF GEOPHYSICAL RESEARCH, VOL. 99, NO. C4, PAGES 7689–7705, APRIL 15, 1994

Mean zonal momentum balance in the upper and central equatorial Pacific Ocean

Eric S. Johnson
Pacific Marine Environmental Laboratory, NOAA, Seattle, Washington

Douglas S. Luther
School of Ocean and Earth Science and Technology, University of Hawaii at Manoa, Honolulu

Abstract. We examine the mean zonal momentum balance in the tropical mid-Pacific using a year of acoustic Doppler current profiler velocities and conductivity-temperature-depth profiler densities from the Hawaii-to-Tahiti Shuttle Experiment. All significant contributions from the mean, annual cycle, and higher-frequency flow fields are determined with the exception of the vertical stresses. We find that even neglecting vertical stresses, the zonal momentum equation is in rough balance at 90–117-m depth at all latitudes from 4°S to 10°N. While the formal error bars are large, this rough balance is reproducible over four to five independent latitudes and so is probably real. The balance at 90-m depth is geostrophic to within 5° of the equator. Closer to the equator, meridional mean convergence and meridional eddy stresses contribute important forces to balance the mean pressure gradient. Nearer the surface, the zonal momentum equation is dominated by eastward pressure gradients near the equator and eastward Coriolis forces from a strong, northward Ekman flow poleward of 2°N. In the vertical integral these forces roughly balance the surface wind stress; thus vertical stresses suffice to close our momentum budget. We conclude that on average vertical stresses arising from the wind forcing do not penetrate deeper than 90 m into the tropical ocean. This contradicts an earlier study of the equatorial zonal momentum budget but is consistent with turbulent dissipation measurements on the equator. Previous findings of stronger, deeper dissipation on the equator are probably due to the stronger, deeper mean shear there rather than to a locally altered stress profile. Vertical turbulent viscosities derived from our observations agree with previous observations on the equator but contradict the conventional, Richardson number parameterization off the equator.

1. Introduction

The prevailing balance of forces in the midlatitude thermocline is geostrophic, where the Coriolis force is balanced by the horizontal pressure gradient. Above the thermocline, in the top few tens of meters of the water column, the vertical stress produced by the surface wind is balanced by the Coriolis force in a surface wind drift or Ekman layer. At the equator, however, the horizontal component of the Coriolis force vanishes, and the westward stress due to the trade wind is expected to penetrate more deeply into the ocean to balance the thermocline pressure gradient directly [e.g., *Stommel*, 1960]. Numerous model calculations have explored this transition from midlatitude to equatorial dynamics. While many models succeeded in reproducing reasonable mean currents, little consensus was achieved over the exact dynamics involved and the specific roles of advection and eddy processes. Furthermore, the dynamical balances are likely to vary zonally, as emphasized recently by *Wacongne*'s [1989, 1990] analyses of numerical model simulations.

The observational resolution of the relative importance of the various forces in the zonal momentum equation has been hampered by the difficulty and expense of gathering adequate data. The earliest efforts served mostly to define the magnitude of the problem. *Knauss* [1966] estimated the sizes of the various steady state momentum terms and found them all to be important. *Taft et al.* [1974] confirmed this result and further found that the local acceleration is important, being as large as the pressure gradient itself over a 25-day period.

More quantitative results awaited the collection of larger volumes of data, such as during the 15-month long effort of the North Pacific Experiment (NORPAX) Hawaii-to-Tahiti Shuttle (hereinafter referred to as the Shuttle Experiment). *Mangum and Hayes* [1984] used the equatorial conductivity-temperature-depth (CTD) profiles at 150°W from the Shuttle Experiment and at 110°W from the Equatorial Pacific Ocean Climate Study (EPOCS) cruises to estimate the mean zonal pressure gradient and showed that its vertical integral balanced the mean zonal wind stress. *Bryden and Brady* [1985] expanded that analysis by estimating geostrophic transport through the perimeter of a box bounded by the CTD sections along 150°W and 110°W between 5°N and 5°S. After judicious adjustments to the geostrophic velocities to rationalize the deeper flow they added near-surface, Ekman transports estimated from climatological wind stresses and balanced

Paper number 94JC00033.
0148-0227/94/94JC-00033$05.00

the resulting horizontal divergences with a uniform band of upwelling confined to within 3/4° of the equator. Having found both zonal and vertical mean velocities on the equator, they were able to estimate the zonal and the vertical mean advection contributions to the zonal momentum balance and found each to balance about 20% of the surface wind stress.

Bryden and Brady [1989] added to their scheme horizontal eddy stresses measured by moored current meters clustered about the equator. They attributed the residual of their final, equatorial balance between pressure gradient and horizontal advective forces to vertical eddy stress, believing this to be the sole remaining term of importance. This stress arises from the surface wind forcing; and, in fact, the vertical integral of their momentum residual closely matched the climatological wind stress. Their inferred vertical stress, however, was nonzero to depths of over 200 m, therefore requiring that wind stress penetrate deeper than the core of the Equatorial Undercurrent (EUC) which at this location is about 120 m deep.

Such deep penetration of vertical eddy stress is contradicted by more direct estimates of vertical stress derived from dissipation measurements made during later experiments [*Dillon et al.*, 1989; *Hebert et al.*, 1991]. These measurements indicate that turbulent stress penetrates only about 60 m into the ocean. Other mechanisms were proposed which might transport momentum deeper into the ocean, such as internal waves [*Dillon et al.*, 1989; *Wijesekera and Dillon*, 1991], but recent measurements seeking evidence of such processes give no indication that they are significant below the EUC core [*Moum et al.*, 1992].

Subsequent studies of the long-term zonal momentum balance [e.g., *McPhaden and Taft*, 1988; *Wilson and Leetmaa*, 1988] have not been as comprehensive as *Bryden and Brady*'s [1985, 1989] work but have generally confirmed that on the equator the mean wind stress is approximately opposed by the pressure gradient.

The observational studies to date have addressed only the momentum balance on the equator itself, even though model results indicate that the balances prevailing even a few degrees off the equator are likely to be very different. Further, these disparate balances are intimately linked by a strong vertical/meridional circulation and by direct eddy heat and momentum fluxes. Thus the dynamics on the equator cannot be viewed in isolation from those to the north and south. Any attempt to estimate the off-equatorial balances would require accurate measurements of meridional gradients and velocities, which can be neglected on the equator itself by symmetry. Such measurements have hitherto been lacking but were provided on the latter part of the Shuttle Experiment by a ship-borne Doppler current profiler.

We therefore present an expanded analysis of the zonal momentum budget which supersedes the previous work in several important regards. Firstly, all velocities are directly measured and thus unconstrained by prior assumptions or subjective adjustments. Secondly, the contributions of the mean flow, the annual cycle, and the higher-frequency variability are all distinguished and their errors explicitly dealt with. Finally, all momentum terms are calculated over a full range of latitudes, revealing the remarkable meridional structure of the momentum balances near the equator.

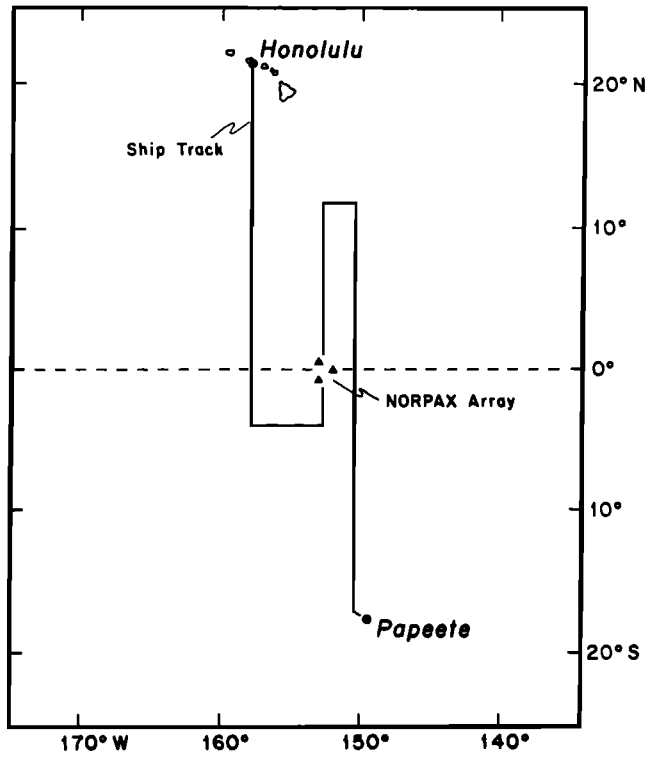

Figure 1. The nominal cruise track during the NORPAX Hawaii-to-Tahiti Shuttle Experiment and the concurrent mooring array. The present analysis uses data from all three longitudes and concentrates on the heavily sampled latitudes between 4°S and 10°N.

2. Data

2.1. The Shuttle Experiment

The NORPAX Hawaii-to-Tahiti Shuttle Experiment occurred between February 1979 and June 1980. It comprised 15 approximately monthly cruises on the nominal track shown in Figure 1 and yielded a succession of north-south sections across the equator along longitudes 158°W, 153°W, and 150°W. CTD profiles to 1000 dbars were collected every degree of latitude or longitude along the cruise track, and profiling current meter (PCM) stations were occupied every degree of latitude between 6°S and 10°N with additional half-degree stations within 3° of the equator. Concurrent acoustic Doppler current profiler (ADCP) data were collected continuously along the ship's track, except for the first few months. This ADCP data collection system was added to the Shuttle Experiment by R. Knox, L. Regier, and D. Cutchin. Since the ship traversed the cruise track in alternate directions, all shipboard data are sampled unevenly in time. In addition to these data a set of three vector-averaging current meter moorings were maintained by R. Knox during the experiment at 0°40'N, 153°W; 0°40'S, 153°W; and 0°, 152°W.

2.2. Acoustic Doppler Current Profiler Measurements

The ADCP instrument returned reliable velocities from depths between 26 and 117 m in 6.5-m depth bins; every second bin is independent. *Johnson* [1987] cleaned the data and converted the raw velocities relative to the ship into absolute velocities relative to the fixed Earth by adding satellite navigation-derived estimates of the ship's motion.

In the present investigation of large scale phenomena we further average the ADCP data over 1°-latitude bins to reduce the navigational noise and match sampling scales with the CTD data. *Johnson et al.* [1988] compared these averaged velocities with concurrent PCM and moored current meter (MCM) data. They found that while the ADCP vertical shears were extremely accurate, the absolute velocities contained large, depth independent noises due to navigational errors. These noise levels are 14 cm/s rms for zonal velocity and 7 cm/s for meridional velocity. While the noise levels are high, they nevertheless account for only a quarter of the observed variance. We also focus our analysis on the most heavily sampled latitudes, between 4°S and 10°N, using 27 sections of data scattered over the three sampling longitudes and over a year of time between July 1979 and June 1980. Additional details of the preparation of ADCP and CTD data are given by *Luther and Johnson* [1990] (hereinafter referred to as LJ).

2.3. Profiling Current Meter Measurements

The PCM measurements were taken by a profiling Aanderaa current meter [*Firing et al.*, 1981] when the ship was stopped on station, whereas the ADCP data used here were taken while the ship was steaming between stations. Nevertheless, the two data sets sampled the same large scale variability, and averaging them would not significantly reduce the geophysical noise but might reduce the instrumental noise. The PCM's instrumental noise, however, is undoubtedly the larger; comparisons with ADCP velocities [e.g., *Johnson et al.*, 1988] show that in the top 100 m alone the PCM measurements have rms errors in integrated vertical shear of over 10 cm/s. Additional errors arise from deeper shears and nonzero velocities in the reference layer. Qualitatively, the PCM mean velocities and consequent momentum quantities appear noisier than the corresponding ADCP quantities; this may explain why the PCM's meridional flow below 180 m is substantially ageostrophic and apparently unbalanced by other forces. Thus we do not average or combine the PCM data with the more accurate ADCP data but use it where appropriate to provide the reader a greater feel for the depth range of particular features.

2.4. Aliasing

The monthly sampling interval of the Shuttle Experiment was sufficient to resolve the mean circulation and its annual cycle, but the higher frequencies are poorly distinguished from one another and are lumped together in our analysis. While this precludes some types of analyses that require frequency separation, the lack of spectral information does not inhibit, for example, estimation of the mean Reynolds stresses that result from the action of all the higher-frequency variability. Furthermore, the statistics we have estimated to study the zonal momentum balance are relatively unaffected by aliasing; at worst, some of the higher-frequency fluctuations will produce small biases of the estimated annual cycle or mean flow contributions. Such biases are accounted for in the error analyses below. A more detailed discussion of aliasing is offered in LJ.

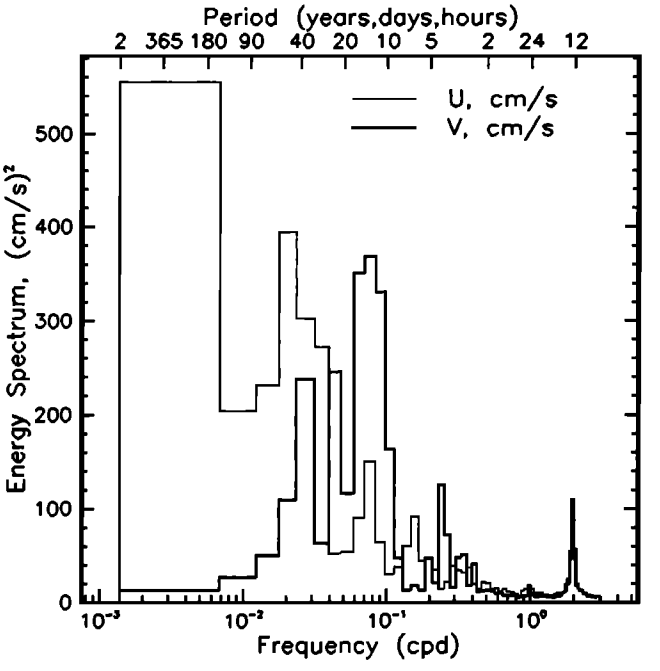

Figure 2. The variance-preserving spectra of horizontal velocity at 0°, 152°W, and 50-m depth. The variability is concentrated in an annual cycle and a higher-frequency band (10–60-day periods).

3. Analysis

3.1. Time Variability and the Multiple Linear Regression

The variability sampled during the Shuttle Experiment can be divided into three frequency bands; the mean flow, the annual cycle, and the high-frequency variability. For brevity the latter are termed the "eddies," although no dynamical interpretation is to be implied by that term. To a first approximation the three bands can be considered distinct in frequency space. Figure 2 shows a variance-preserving plot of zonal and meridional velocity spectra. The annual cycle is dominated by zonal velocity at 1 and 2 cycles per year (cpy), while the energy at the higher frequencies resides mostly at periods shorter than 90 days. Interannual variability is also present in the tropical regions but was not well sampled by the Shuttle Experiment; it appears to be small during this period since time trends are negligible (LJ). Following LJ, we use a multiple linear regression (MLR) to decompose the measured flow variables into the three frequency bands. The mean is specified at each spatial point by a constant and an east-west trend, the annual cycle by the first and second annual harmonics, and the eddy field by the residual of the regression after the lower-frequency terms are removed.

$$P = \langle P(x, y, z) \rangle + P_a(y, z, t) + P^*(x, y, z, t) \qquad (1)$$

Here angle brackets or overbars denote a mean over the year of data, a subscripted a denotes the annual cycle, and a superscripted asterisk denotes the residual eddies; Cartesian coordinates are defined in the usual sense. P represents the pressure relative to 1000 dbar, the maximum depth of the CTD casts. Relations similar to (1) are defined for the velocity components (U, zonal; V, meridional; and W, vertical) and density (ρ). The frequency separation between

the flow fields in both the observations and the formal decomposition allow us to write

$$\langle X_a \rangle = \langle X^* \rangle = \langle X_a X^* \rangle = 0$$

for any variable X.

As in LJ, we ignore zonal variation of the annual cycle since previous studies [e.g., *Meyers*, 1979] indicate that it will be small over the 8° of longitude covered by our study region. A zonal trend in the mean, however, is explicitly recognized. This is in contrast with published statements that the zonal gradients of temperature [*Wyrtki and Kilonsky*, 1984] and velocity [*Johnson et al.*, 1988] in the Shuttle Experiment data were not statistically significant. Wyrtki and Kilonsky apparently confused the standard deviation of temperature with the standard error of its mean, thus underestimating the reliability of the observed gradient. Johnson et al. had not accounted for the annual cycle, which contributes over half of the observed zonal velocity variance (e.g., LJ). Thus the residual variance about their means was about twice that of the present simultaneous fit of means and annual cycles, and their error estimates were correspondingly larger.

3.2. Momentum Equation

Assuming negligible viscosity and no external forcing and using the above frequency band decomposition and orthogonality conditions, the equation for the mean zonal momentum balance becomes

$$\begin{aligned}\frac{\partial}{\partial t}\langle U\rangle = &-\frac{1}{\rho}\frac{\partial}{\partial x}\langle P\rangle + f\langle V\rangle \\ &- \langle U\rangle\frac{\partial}{\partial x}\langle U\rangle - \langle V\rangle\frac{\partial}{\partial y}\langle U\rangle - \langle W\rangle\frac{\partial}{\partial z}\langle U\rangle \\ &- \left\langle V_a\frac{\partial}{\partial y}U_a\right\rangle - \left\langle W_a\frac{\partial}{\partial z}U_a\right\rangle \\ &- \left\langle U^*\frac{\partial}{\partial x}U^*\right\rangle - \left\langle V^*\frac{\partial}{\partial y}U^*\right\rangle - \left\langle W^*\frac{\partial}{\partial z}U^*\right\rangle \end{aligned} \tag{2}$$

Here we have not added the continuity equation to commute velocity with the gradient operators in the advection terms, as is often done to give a flux gradient form to the Reynolds stresses. In general, our data do not sample zonal and meridional gradients simultaneously, so continuity holds only in the statistical mean; thus adding continuity to an advection term introduces additional oceanic as well as instrumental noise, both of which can be substantial (LJ).

The long-term time derivative on the left-hand side of (2) is small over an annual average (note, however, that we have the mean of 27 stochastic samples scattered over a year rather than an average of continuously sampled data). On the right-hand side there is the pressure gradient and the Coriolis acceleration composing the geostrophic balance on the first line, the three components of mean flow advection on the second line, the annual cycle advection terms on the third (recall that the zonal gradients of the annual cycle were explicitly neglected in (1)), and finally the eddy advection terms. Of these terms we can measure with the present data all but the two terms due to time dependent vertical advection. The annual cycle vertical advection term is certainly smaller than the corresponding mean flow term; annual vertical velocities are no larger than the mean (or the equatorial upwelling would reverse every year), and annual zonal velocities are several times smaller than mean flow velocities and have very similar vertical scales. The eddy vertical advection term is likely dominated by turbulent stresses at very small vertical and horizontal scales. While the vertical turbulent stress divergences are not measurable with the present data, their vertical integral can be estimated; assuming much smaller turbulent stresses below the study region and negligible radiation of momentum through internal waves, the vertical integral of the turbulent advective forces must equal the imposed surface wind forcing.

In the interest of brevity we will refer to the various advective components of (2) chiefly by the advecting flow field; thus the mean eddy meridional advection of meridional gradients of eddy zonal velocity (the second to the last term of (2)) will be rendered "the eddy meridional advective term."

3.3. Errors

Errors in our observed mean quantities arise from two sources, instrumental errors and geophysical errors. The latter arise since we do not have a true average over a year of data but rather a mean of stochastic, independent sections scattered throughout the year (LJ). In such a case the statistics of the high-frequency variability are incompletely known, and that variability aliases into the annual cycle and mean fields to produce uncertainty in those statistics as well. The high-frequency variability is roughly independent of depth (LJ) over the range measured, as is the instrumental noise (see section 2.2). Thus the noises in our analysis will be, to a first approximation, depth independent.

Throughout the analysis we will present rms errors for representative terms. We have estimated errors both parametrically (e.g., LJ) and using the bootstrap method (see appendix) with similar results. The error estimates presented here are the bootstrap errors. The appendix gives additional details and a comparison of the error calculations.

To the extent that a stochastic quantity is roughly Gaussian in distribution, 1.96 rms errors in either direction from its mean represent 95% confidence intervals. As in LJ, we will consider quantities distinguished from zero by 2 rms errors to be significantly observed, although less significant quantities will also be noted when of particular scientific interest. It is important to note that the rms errors apply only to the uncertainty with which a given quantity is observed by the present data set for the year sampled. They contain no information regarding the interannual stability or stationarity of that quantity.

4. Time Independent Fields

4.1. Mean Fields

To facilitate the interpretation of the following results, we first familiarize the reader with the strong, highly structured mean currents of the study region. Figure 3 shows the mean ADCP velocity and CTD density fields as estimated using the MLR (section 3.1). These mean fields are virtually indistinguishable from those of LJ, who neglected the mean zonal trend included in the present MLR. Briefly, zonal

velocity shows a typical section of the near-equatorial currents. The eastward velocities centered on the equator compose the Equatorial Undercurrent (EUC). Overlying and surrounding the EUC are the westward velocities of the South Equatorial Current (SEC). Centered at 6°N is the North Equatorial Countercurrent (NECC), whose eastward velocities are separated from the EUC by the relatively strong, northern hemisphere branch of the SEC which we will term the SECN. Finally, north of 9°N we see the edge of the westward flow associated with the North Equatorial Current (NEC). The rms errors of mean zonal velocity are no more than 5 cm/s (not shown).

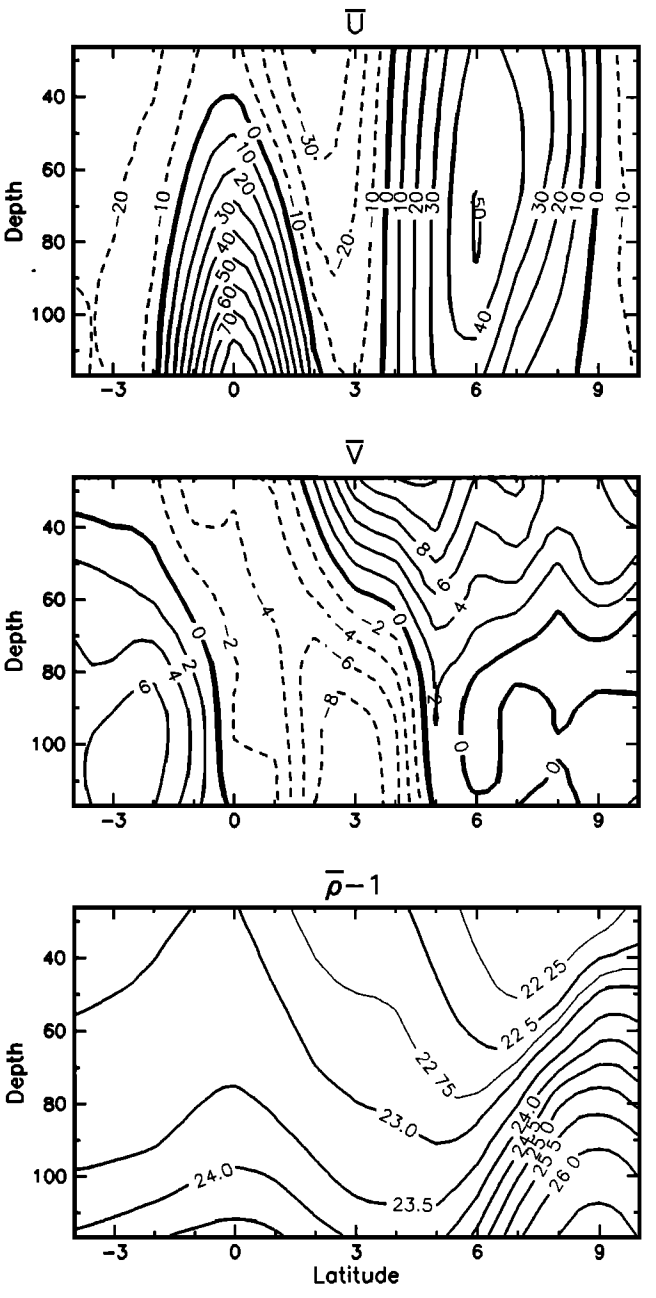

Figure 3. The longitude-averaged, fitted means of horizontal velocity (in centimeters per second) and in situ density (10^{-3} g/cm^3) for the study period. All major features are significant at 95% confidence. (top) Zonal velocity shows the very strong currents of the tropics. (middle) Meridional velocity has a convergence on the equator below about 50-m depth and a surface divergence at about 2°N with a strong northward flow at 3°–6°N. These and all subsequent velocities are acoustic Doppler current profiler (ADCP) measurements, unless otherwise specified. (bottom) Density is in close (but not exact) geostrophic balance with zonal velocity only below 70 m.

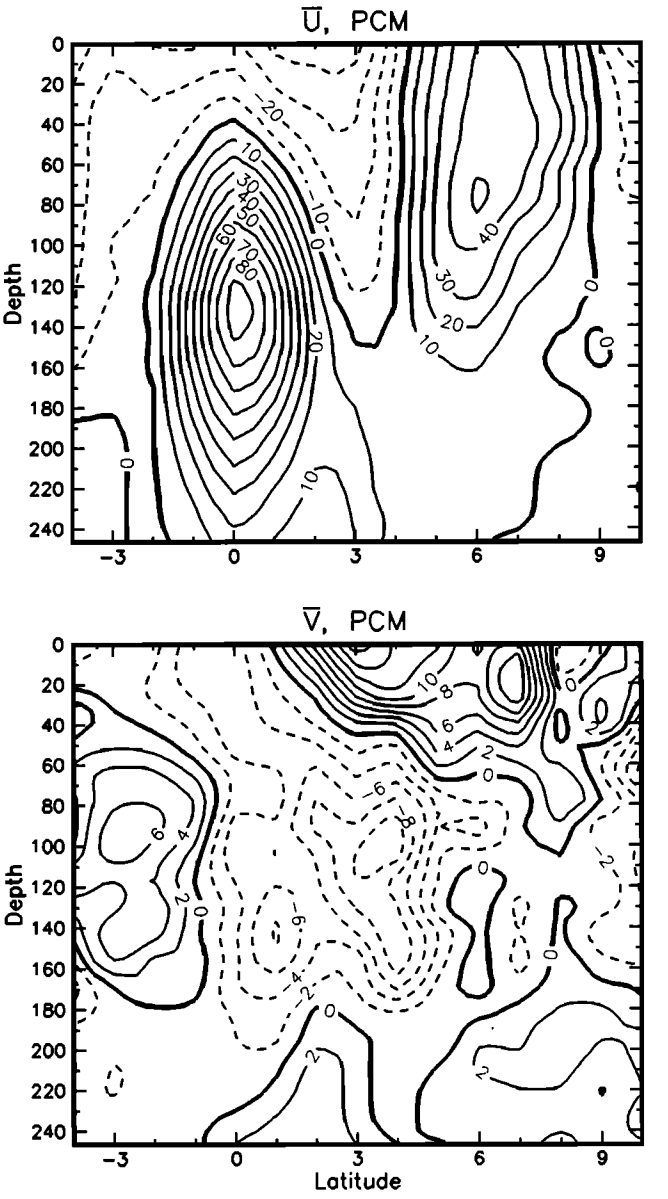

Figure 4. As in Figure 3, but for profiling current meter (PCM) velocities. Unlike for the ADCP data in Figure 3, the depth ranges of the strong, near-surface zonal currents and their associated meridional circulations are evident.

Mean meridional velocity is much smaller than mean zonal velocity, and its estimated errors of 4 cm/s or less are proportionately larger. Nevertheless, the convergence above the EUC core is significant at 2 rms errors. The overlying, wind-driven surface divergence is also statistically significant, and its asymmetry about the equator is a robust feature of this data set, although the exact location of the velocity zero is in doubt (see section 6.7 for further discussion). The strong, surface current flowing northward

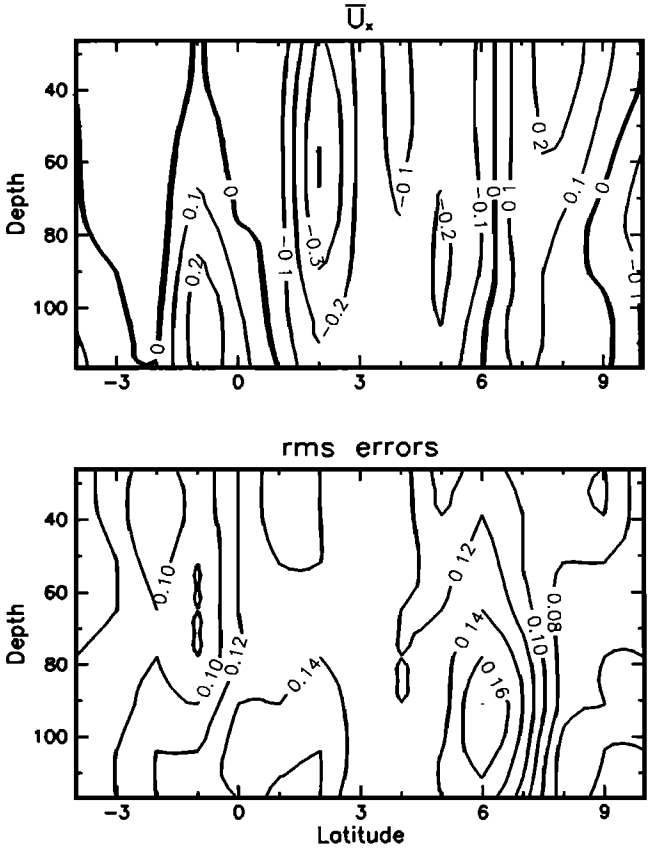

Figure 5. The mean zonal trend of zonal velocity in 10^{-6} s^{-1} and rms errors. All the major features are observed with good statistical significance.

from the equatorial regions is highly significant and is also seen in numerical models of the region [e.g., *Philander et al.*, 1987; D. E. Harrison, unpublished manuscript, 1993]. The results of succeeding sections will show that the Coriolis forces associated with this flow oppose the westward stresses of the trade winds in a familiar Ekman balance.

Figure 4 shows the equivalent means of concurrent PCM data, which we use to show mean flow structures beyond the ADCP's restricted depth range. The velocity core of the EUC is at about 135-m depth, just below the ADCP's depth limit of 117 m. Below this depth the currents of the SEC and NECC are much reduced. Similarly, in the mean meridional circulation the subsurface convergence on the equator is confined to above approximately 180 m. The deeper, northward velocities in the PCM means are likely spurious, as mentioned in section 2.3. Note, also, that the PCM means exhibit more small scale variability than the ADCP means, especially in meridional velocity, suggesting that the PCM data have larger geophysical and/or instrumental noise levels than do the ADCP data.

The mean density field, shown in Figure 3 (bottom), is also typical of the region; the isopycnals bowing upward on the equator are in approximate thermal wind balance with the negative vertical shears of the EUC [e.g., *Lukas and Firing*, 1984], while the troughing isopycnals to the north reflect the change in sign of the vertical shears between the SECN and the NECC.

4.2. Zonal Gradients

Figure 5 shows the zonal gradient of zonal velocity from the MLR fit. The three largest extrema (in the EUC, SECN, and NECC) are all statistically significant at 95% confidence and are in accord with prior expectations. Positive values prevail above the EUC core, since that current surfaces as it flows eastward. The negative values in the SECN imply that it is weakening as it flows westward, possibly a very localized consequence of interaction with Christmas Island (2°N, 157°W), which is centered in the SECN close to the westernmost leg of the Shuttle Experiment track. Negative values in the southern parts of the NECC and positive values to the north indicate that it is shifting northward as it flows to the east, consistent with the dynamic topography of the tropical Pacific [*Kendall*, 1970; *Taft and Kessler*, 1991].

The observed zonal pressure gradient force in Figure 6 is highly significant. The force is strongest within 4° of the equator with a local minimum right on the equator. Poleward of 5°N, the sign of the mean gradient is uncertain. The pressure gradient force is the first term of the zonal momentum balance in (2). We present all such terms as accelerations in units of 10^{-6} cm/s^2.

The zonal gradients shown are the local gradients appropriate to momentum calculations in the Shuttle Experiment region itself; nevertheless, they are quite comparable with the broader scale gradients defined by EPOCS moorings at 140°W and 110°W. In the 4-year means of *Johnson and McPhaden* [1993] the mean zonal velocity gradient on the

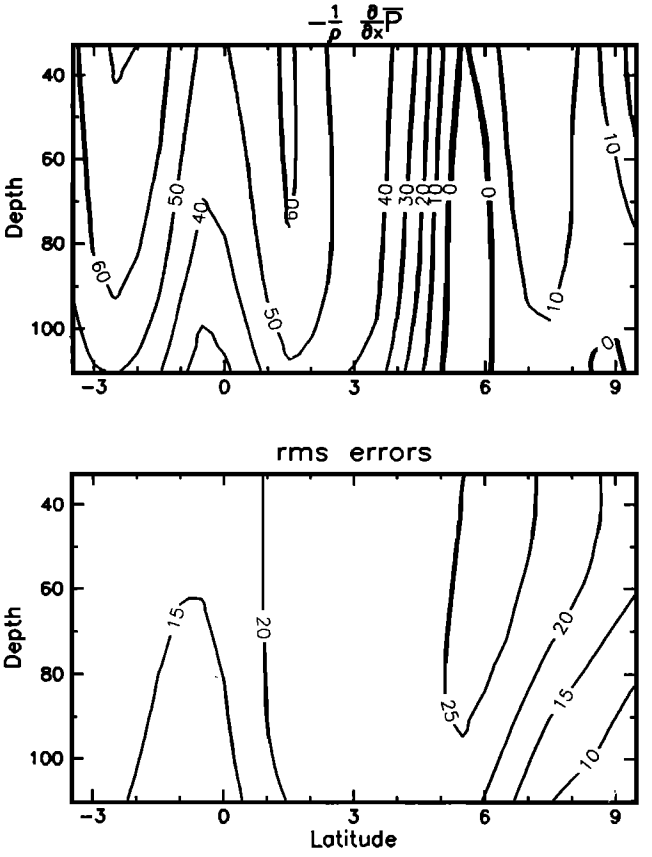

Figure 6. The mean zonal pressure gradient force in 10^{-6} cm/s^2 and rms errors. Note the large, eastward values within 4° of the equator.

equator has a maximum of 0.13×10^{-6} s^{-1} at 45-m depth, comparable with our values considering the shallower depth of the EUC in their more easterly region. Similarly, their mean pressure gradient force varies from 60×10^{-6} cm/s^2 at 26-m depth to 10×10^{-6} cm/s^2 at 117-m depth, comparable with our values shown in Figure 6.

4.3. Vertical Velocity

Having determined both components of mean horizontal convergence, we can use the continuity equation to estimate the mean vertical convergence; then by linearly extrapolating that convergence to the surface and integrating it downward, we can find the mean vertical velocity. In general, horizontal convergence is dominated by the meridional component; zonal convergence partially cancels this contribution but does not alter the broad structure of the field. The resulting vertical velocity is shown in Figure 7. "Equatorial" upwelling is strongest just north of the equator because of the location of the surface divergence around 2°N. Fluid accumulating near the equator in the subsurface convergence upwells into this divergence north of the equator, but farther to the south it must be downwelled. Similar downwelling occurs where the northward surface current slows from 4°N to 7°N; but as the surface current accelerates again north of 7°N, upwelling is reestablished. The estimated errors of this calculation are large, since the horizontal convergences cancel to some degree but their errors add. To mitigate this, we have averaged mean vertical velocity over 3° latitude (see appendix); yet still the structures of mean vertical velocity are only poorly distinguished from zero.

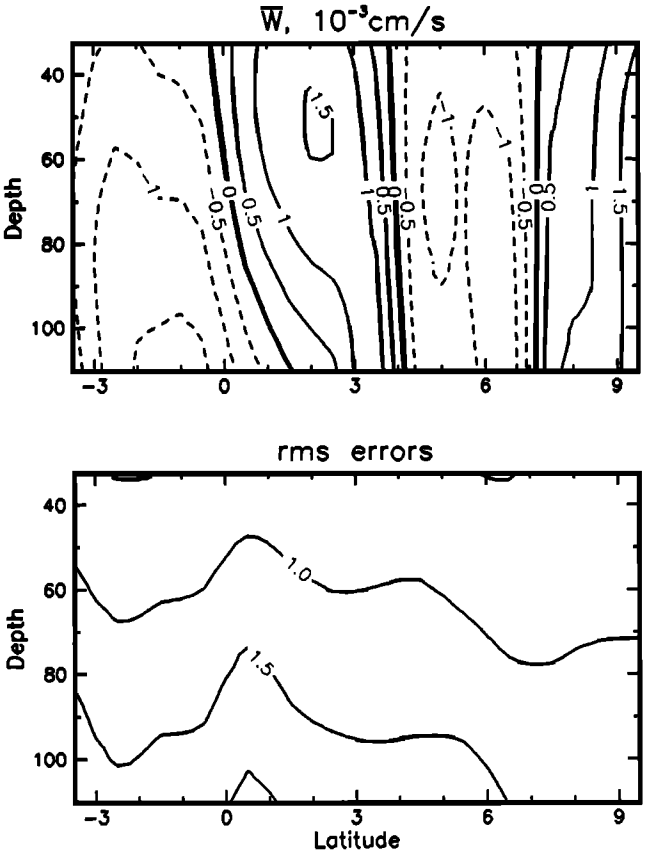

Figure 7. Mean vertical velocity derived using the continuity equation in 10^{-3} cm/s and rms errors. Note the near-surface upwelling at and north of the equator with downwelling to the south and below.

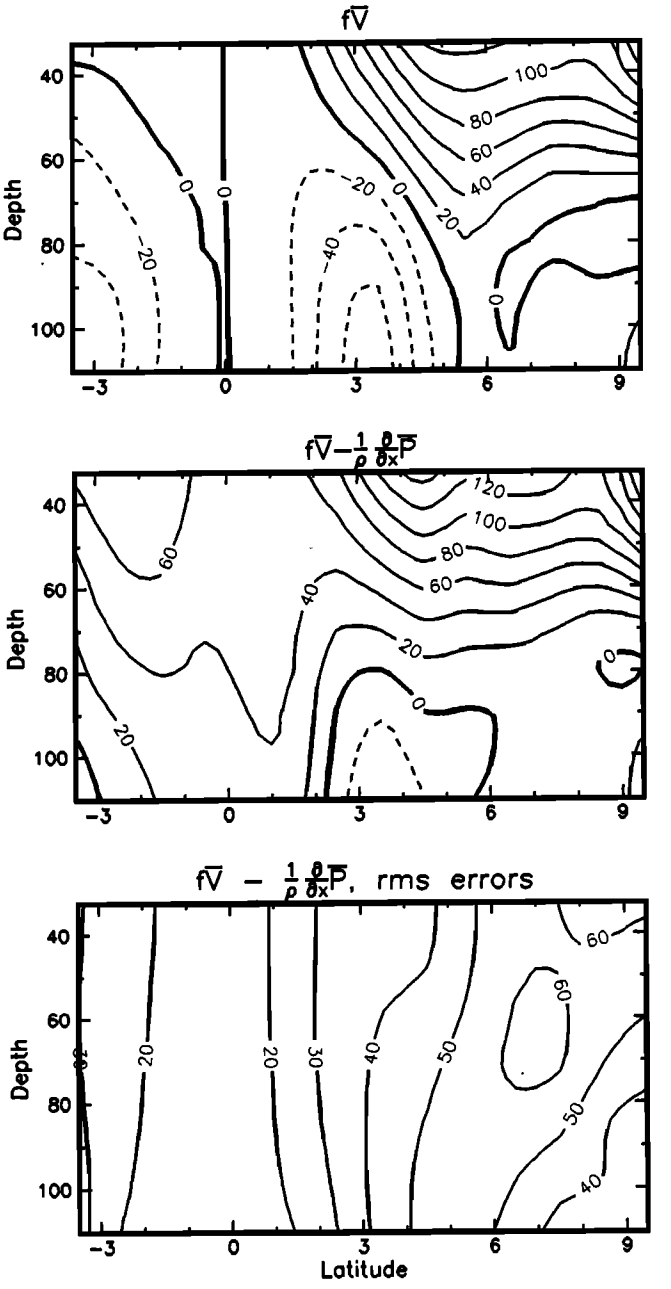

Figure 8. (top) The Coriolis force in 10^{-6} cm/s^2 with the (middle) residual from the geostrophic balance and (bottom) its rms errors. The westward forces produced by the meridional convergence on the equator just balance the pressure gradient below 90-m depth at 3° and 4° from the equator, while nearer the surface the pressure gradient and Coriolis force combine to give eastward forces at all latitudes.

5. Zonal Momentum Balance

The zonal momentum budget comprises a number of processes having completely different dynamics. To emphasize this point, we present the terms in groupings of similar dynamics as follows: (1) the geostrophic balance, made up of

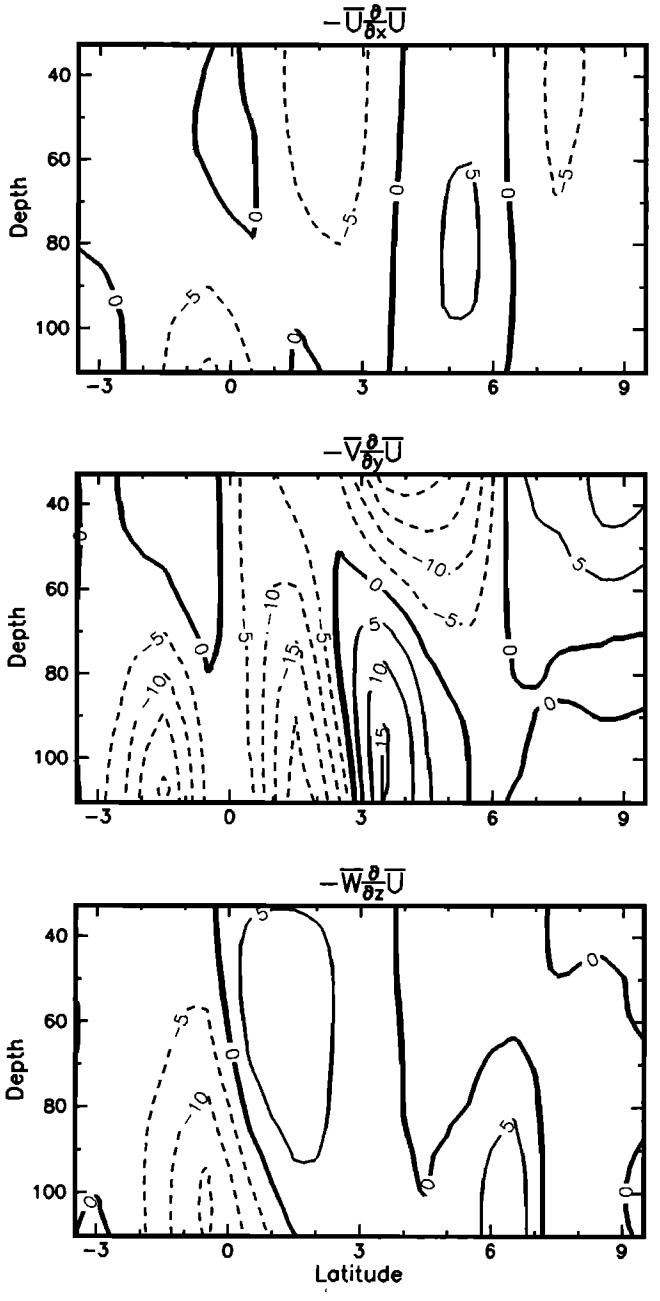

Figure 9. The forces due to (top) mean zonal, (middle) meridional, and (bottom) vertical advection of mean zonal momentum in 10^{-6} cm/s^2. Meridional advection is the largest, advecting westward momentum into the fringes of the EUC, eastward momentum from the NECC into the SEC at 3°–4°N, and westward momentum into the NECC near the surface.

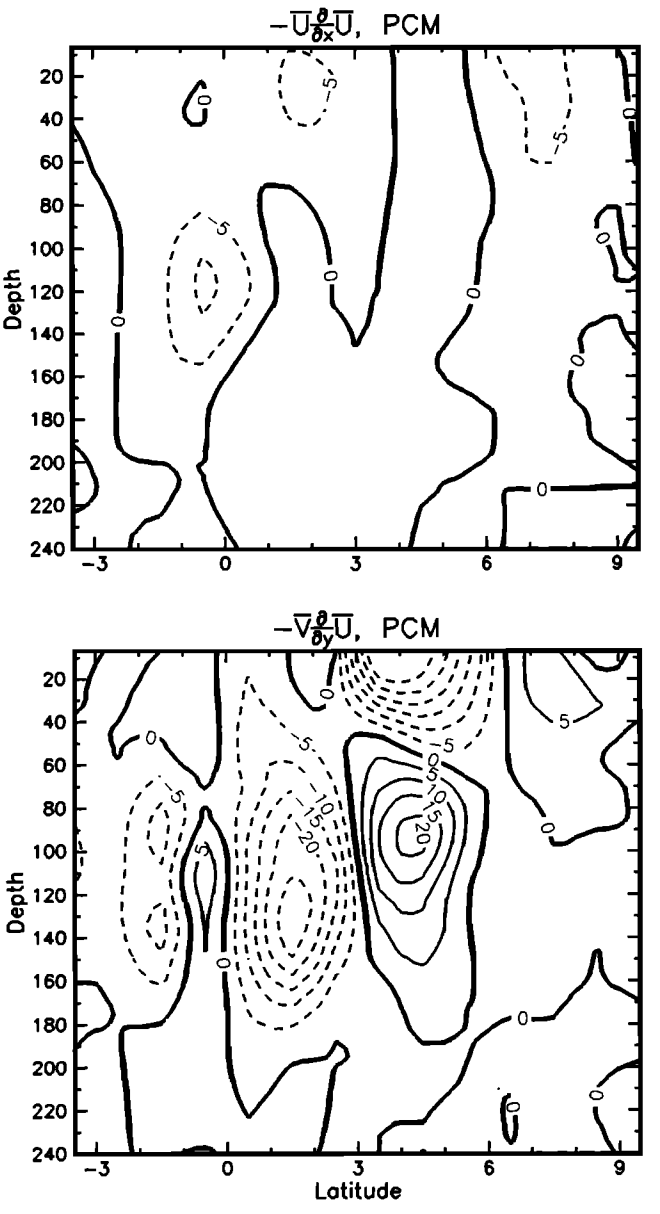

Figure 10. As in Figure 9, but for PCM mean horizontal advection. Note that large values do not extend much below the depth range of the ADCP.

the pressure gradient force introduced above and the Coriolis force; (2) the mean flow advective forces; and (3) the advective forces due to time dependent flows.

5.1. Geostrophic Balance

The Coriolis force shown in Figure 8 (top) reflects the mean meridional velocities and the sign change of the Coriolis parameter f on the equator. The subsurface equatorial convergence contributes westward forces within 5° of the equator, while the surface poleward flow contributes stronger eastward forces to the north (as the Coriolis parameter increases). The sum of the pressure gradient force (Figure 6) and the Coriolis force is dominated by the eastward Coriolis forces of the near-surface flow and the eastward pressure gradient near the equator (Figure 8, middle). The westward Coriolis forces from the subsurface equatorial convergence are insufficient to balance the pressure gradient, except at 90-m to 110-m depth and 3° to 4° from the equator. There the equatorward convergence is in rough geostrophic balance. The rms errors of the geostrophic balance are quite large in the north due to the poleward increase of the Coriolis parameter.

5.2. Mean Flow Advection

The mean flow zonal advection of zonal momentum (Figure 9, top) is relatively small, but its negative extrema are all

significant at over 2 rms errors. These westward forces help offset some of the prevailing pressure gradient near the equator. The eastward forces in the NECC are only about 1.5 rms errors from zero.

The mean flow meridional advective term (Figure 9, middle) is larger in magnitude. All its major features are significant at about 95% confidence. The strong convergence above the core of the EUC (see Figure 3) advects westward momentum from the surrounding SEC into the fringes of the EUC. This advection does not reach to the equator, however, since both mean meridional velocity and the mean meridional gradient of zonal velocity vanish there. At 3° to 6°N, eastward momentum is being advected southward from the center of the NECC below 65-m depth, while westward momentum is being advected northward by the near-surface flow above. The surface flow continues north past the center of the NECC, advecting eastward momentum into the NEC beyond.

For completeness we show in Figure 9 (bottom) the mean vertical advective contribution, although owing to the large errors in vertical velocity, this term is of lesser statistical significance. The upwelling just north of the equator advects eastward momentum upward into the SEC, while the downwelling below and to the south subducts westward momentum into the EUC below. None of the observed values is particularly large compared to the dominant terms of the zonal momentum balance.

To illustrate the approximate depth limits of the maxima shown in Figure 9, we present in Figure 10 the mean flow horizontal advective terms from the corresponding PCM data. Although the exact values are somewhat different, the PCM results indicate that the ADCP depth range extends approximately to the subsurface extrema of these forces and that they diminish to insignificance by about 180-m depth.

The sum of the ADCP mean flow advective forces is shown in Figure 11; it is dominated by the meridional advection component and has very similar statistical significance.

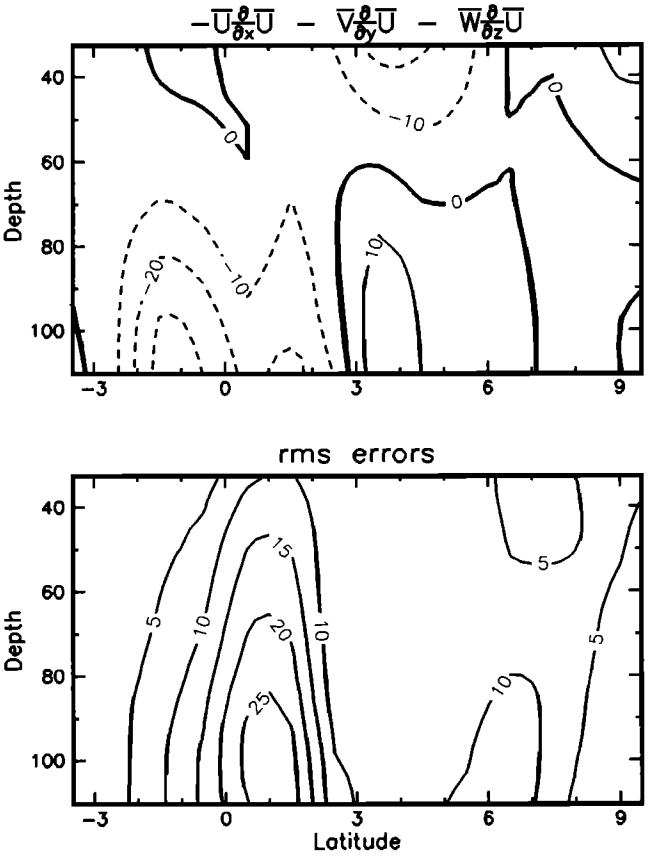

Figure 11. The sum of the mean advective forces of Figure 9 and rms errors. Westward forces of moderate magnitude exist below 60-m depth near the equator with shallow westward forces and deeper eastward forces to the north.

5.3. Advection Due to Time Dependent Flows

The eddy meridional advective term in Figure 12 (bottom) is the largest of the time dependent flow advective terms in (2) that we can directly estimate. This stress arises from the familiar tropical instability waves as they extract energy from the meridional shear between the EUC and the SECN (e.g., LJ). The stress contributes substantial westward forces in a narrow band almost centered on the equator (opposing the strongest flows of the EUC) and eastward forces in a broader band centered at 3°N (principally opposing the westward flow of the SECN). Both extrema are more than 1.5 rms errors from zero.

The eddy zonal advective contribution in Figure 12 (middle) produces only small forces, westward in the vicinity of the equator and eastward around the NECC. Nevertheless, the westward forces near the equator are statistically significant at over 2 rms errors and are consistent with the expected eastward increase in eddy variability [e.g., *Halpern et al.*, 1988]. It is of interest to note that the zonal eddy stress term, while of little importance in the mean momentum budget, has a much larger role in the eddy energy budget; its contribution there is fully half as large as that of the more celebrated meridional stress term (D. S. Luther and E. S. Johnson, manuscript in preparation, 1994).

The annual cycle meridional advection contribution (Figure 12, top) is generally small and not significant; the extremum at 3.5°N is the most significant at 1.3 rms errors.

The sum of the time dependent flow contributions is presented in Figure 13. As for mean flow advection, the meridional eddy advection term dominates the sum. The maximum westward forces near the equator are significant at 1.6 rms errors and the eastward forces to the north at 2.1 rms errors. A comparable sum derived from the PCM data confirms that the observed features have diminishing values below the depth range of the ADCP data (Figure 14). This is consistent with the strong surface intensification of both the instabilities [*Halpern et al.*, 1988] and the annual cycle (R. A. Knox et al., manuscript in preparation, 1994).

5.4. Summed Zonal Momentum Budget

While the structures of the individual components of the zonal momentum balance are of interest, it is not until they are summed that the significance of those structures can be seen and their contributions to the whole understood. As an aid to such understanding, we cumulatively sum the dynamical groups in the order presented above, which is to say from the largest and most broadly important terms to the smallest and most localized.

The largest forces are those of the pressure gradient and the Coriolis force. Recall that within 4° of the equator the

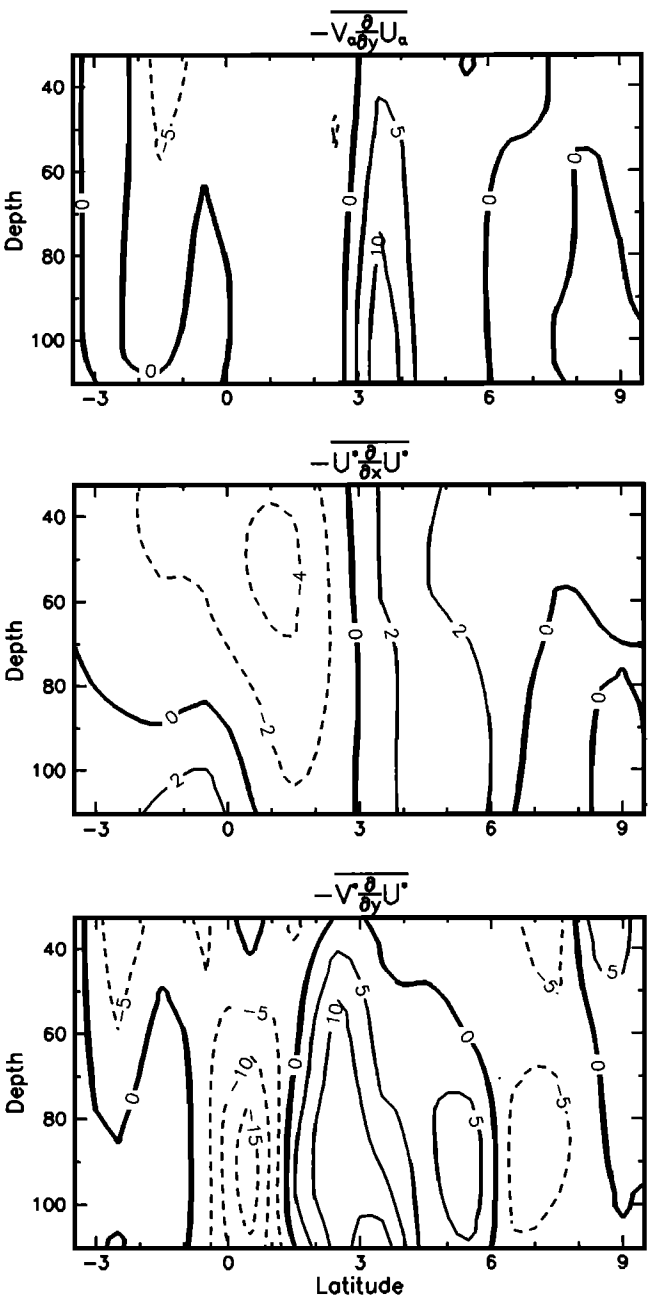

Figure 12. The mean forces due to (top) annual cycle meridional, (middle) high-frequency zonal, and (bottom) high-frequency meridional advection of zonal momentum in 10^{-6} cm/s^2. The annual cycle term is small and not significantly observed. Both high-frequency terms are significant at 95% confidence, but only meridional advection is consequential. It contributes westward forces in the center of the EUC on the equator and eastward forces to the north, mostly due to the stresses of the tropical instability waves.

pressure gradient force (Figure 6) was strongly eastward, and that the Coriolis force (Figure 8) opposed it to achieve a rough geostrophic balance at 90–110-m depths, 3°–4° from the equator. Closer to the equator and nearer to the surface, the eastward pressure gradient force remained dominant, while to the north the eastward Coriolis forces of the strong, poleward flow dominated.

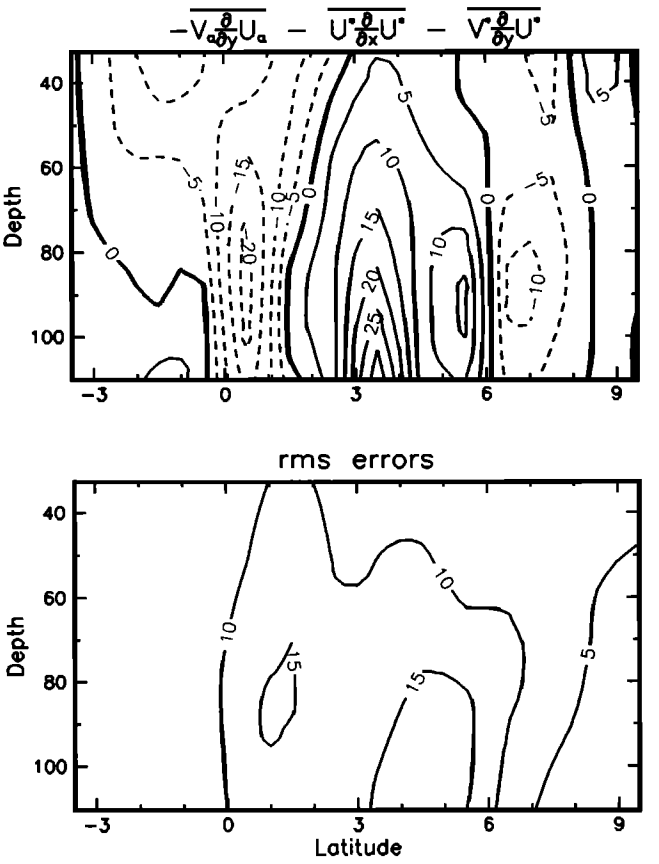

Figure 13. The sum of the time dependent flow advective forces of Figure 12 and rms errors. The high-frequency meridional advective term dominates.

We next include the forces due to mean flow advection, i.e., the second line of (2). Recall from Figure 11 that the net effect of these were smaller, westward forces within 3° of the equator and below 50-m depth and also some near-surface

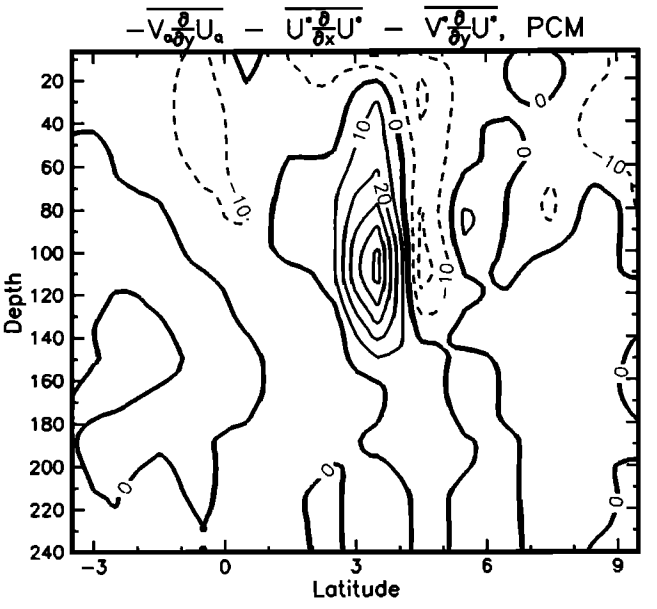

Figure 14. As in Figure 13, but for the PCM velocities. As before, the ADCP has captured most of the relevant variability.

westward tendencies and deeper eastward tendencies from 3°N–6°N. Adding these to the residual from geostrophy gives the mean flow zonal momentum residual shown in Figure 15 (top). Note that below 90-m depth the mean flow advective forces have completely balanced the residual pressure gradient (i.e., Figure 8, middle) south of the equator. The shallower, eastward forces of pressure gradient and Coriolis force remain unopposed.

Finally, we include the time dependent flow advective forces. Dominated by the eddy fluxes of the tropical instability waves, these terms contribute small forces below 50-m depth; westward between 0°N and 1°N and eastward from 2°N to 6°N. Adding these to the previous sum just balances the residual forces below 90-m or 100-m depth, producing a final mean momentum budget residual shown in Figure 15 (middle).

The remarkable result is that despite the large latitudinal variability of its component terms, the mean zonal momentum budget (exclusive of vertical stresses) is in very close balance below 90-m depth at all latitudes in our study region. The implications of this singular observation will be discussed in the section 6 after a consideration of the large errors of the calculation. Note, too, that the Coriolis force of the near-surface, northward flow (refer to Figures 3 and 8) is unopposed by any other measured forces. In the discussion we will show that it is approximately balanced by the surface wind forcing via vertical stresses and hence that this flow has the familiar dynamics of an Ekman layer. What has not been previously observed, however, is that the mean Ekman layer extends downward into the shoaling, mean thermocline north of 7°N (compare Figures 15 and 3). This appears to be more than an artifact of the averaging process, which blurs the boundaries of both the thermocline and the near-surface flow as they fluctuate in depth over the course of the year; individual profiles, though dominated by strong, vertically coherent eddy velocities, nevertheless often show the shear at the bottom of the longer-term, near-surface flow penetrating into the thermocline around 9°N. These upper thermocline velocities are not geostrophically balanced in the mean, since the pressure gradient force and the Coriolis force there are of the same sign (Figures 6 and 8).

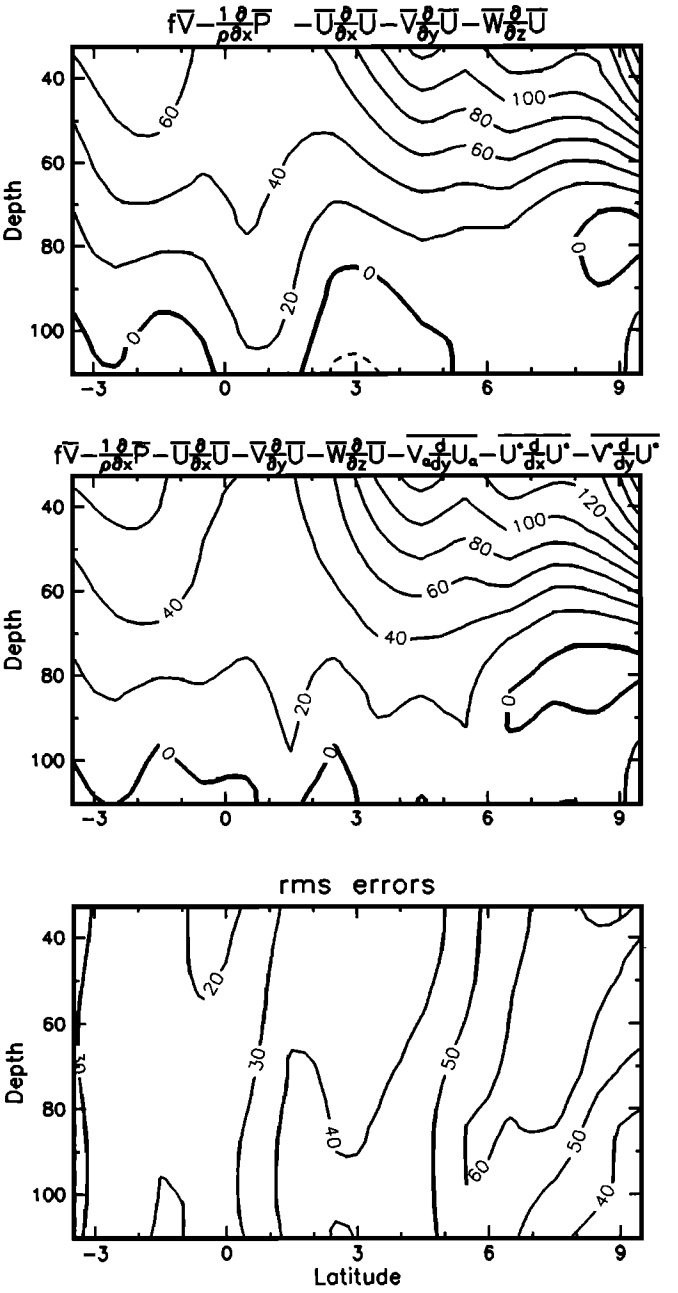

Figure 15. Cumulative sums of the components of the zonal momentum equation. (top) The mean flow balance, comprising the geostrophic balance from the middle panel of Figure 8 and the mean flow advective contributions from Figure 11. Below 90-m depth the mean advective contributions cancel much of the ageostrophic pressure gradient within 3° of the equator. (middle) The mean flow balance above plus the time dependent flow's horizontal advective forces from Figure 13. The latter tend to cancel the residual pressure gradient on the equator itself. The result is a complete zonal momentum balance below 90-m depth at all latitudes. (bottom) Errors for the entire sum.

6. Discussion

6.1. Statistical Significance of the Observed Balance

The formal error bars on the zonal momentum budget of Figure 15 are large relative to the budget residual itself; in fact, only at and south of the equator are the small residuals below 90-m depth statistically distinguished from the unbalanced, near-surface forces. Nevertheless, the observed residuals below 90-m depth are within half a standard error of zero at all latitudes in the study region. Given that the meridional decorrelation scale is about 3° latitude (LJ), we have four or five independent samples in latitude. The chance of one normally distributed variable (i.e., the momentum residual) being within 0.5 standard errors of zero is 38%; but the chance of four independent samples of that variable being so small is only 2%. Thus it is highly likely that our small, observed residuals are not coincidental but in fact are a reflection of a true balance in the underlying, oceanic dynamics.

6.2. Momentum Budget Residual Versus Wind Stress

The term which we have neglected so far in (2) is the vertical eddy stress divergence; presumably, this force closes our momentum equation by balancing the observed momentum residual of Figure 15. In section 3.2 we mentioned that the vertical integral of the vertical stress diver-

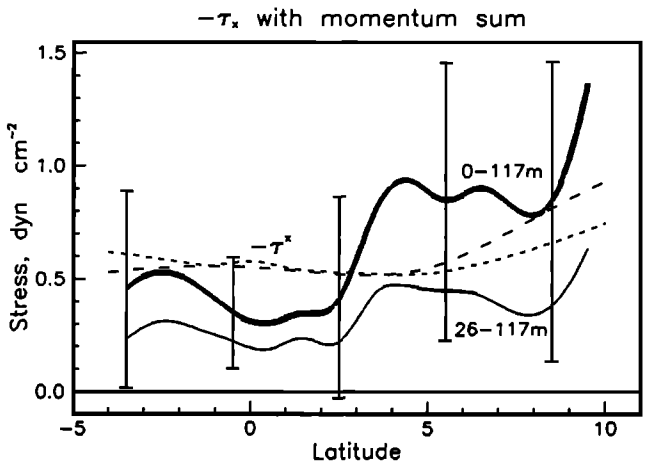

Figure 16. The vertical integral of the zonal momentum residual (Figure 15, middle), compared to the surface wind stress. The integral of Figure 15, shown as the light, solid curve, undercompensates the wind stress. Adding the estimated contribution above 26-m depth produces a closer comparison (dark, solid curve) for which rms errors are shown. The stress estimates are derived from *Sadler et al.*'s [1983] surface wind estimates from cloud motions (long-dashed curve) and *Stevenson*'s [1982] shipboard wind measurements (short-dashed curve).

gence should equal the applied surface wind stress. If (2) holds, then by reflexivity the vertically integrated momentum residual must balance the surface wind stress. From Figure 15 we see that substantial stress divergences are not needed below 90-m depth to balance the zonal momentum equation; we assume that at this depth the vertical stresses themselves are small and thus that the momentum residual below is small as well. Then we may integrate the observed residual upward from the bottom of Figure 15 (middle) and compare the resulting net force on the water column to the negative of the observed wind stress.

Figure 16 (dashed curves) includes two independently measured estimates of wind stress averaged over the study period. Those of *Stevenson* [1982] stem from ship wind observations collected on the Shuttle Experiment cruises, while those of *Sadler et al.* [1983] are satellite observed cloud motions extrapolated to the surface using climatological wind shears. The two estimates agree reasonably well. Compared to these is the integrated momentum residual of Figure 15 (light, solid curve) from 117-m to 26-m depth. The resulting force is everywhere too small. This is not surprising, since we are missing the region above 26 m which is dominated by strong, eastward pressure gradients and Coriolis forces.

Concurrent PCM data indicate that meridional velocities above 26 m can be reasonably estimated by linearly extrapolating from the shallowest velocities in the ADCP depth range. Repeating our calculation with ADCP velocities extrapolated to the surface gives an extended momentum residual whose vertical integral is shown in Figure 16 (dark, solid curve). This integral brackets the wind stress more closely, but the agreement over latitude is only approximate, being within a factor of 2. There is a substantial shortfall of eastward forces in the near-equatorial regions, undercompensating the westward wind stress; north of 9°N and between the centers of the SECN and NECC there is overcompensation. A too strong Ekman flow could result in the overcompensation, because away from the equator the calculation becomes very sensitive to small errors in mean meridional velocity; at 9°N, even a 1 cm/s error contributes a quarter-dyne of force over the 117-m integration range (recall from section 3.3 that errors are roughly depth independent). Owing to the profusion of forces contributing to the momentum balance near the equator, we can offer no insight to the shortfall there. Note again that the formal error bars (shown only for the 0–117-m integral) are large and appear to overstate the uncertainties of the calculation since the agreement between wind stress and integrated momentum residual is everywhere within 1 standard error.

6.3. Vertical Structure

The important difference between the results of our study and that of *Bryden and Brady* [1985, 1989] is our finding of a rough momentum balance below 90-m depth, irrespective of vertical stresses. Bryden and Brady found no such balance anywhere above 200 m (see Figure 17) and therefore required vertical stresses to penetrate deeply into the ocean to close their momentum balance. The forces found above the thermocline are roughly comparable between the two studies, although some differences arise from the different longitude bands of the studies; for example, Bryden and Brady's eddy stresses are stronger than ours, commensurate with their location in the longitudinal maximum of eddy variability [e.g., *Halpern et al.*, 1988]. Yet eddy stresses are

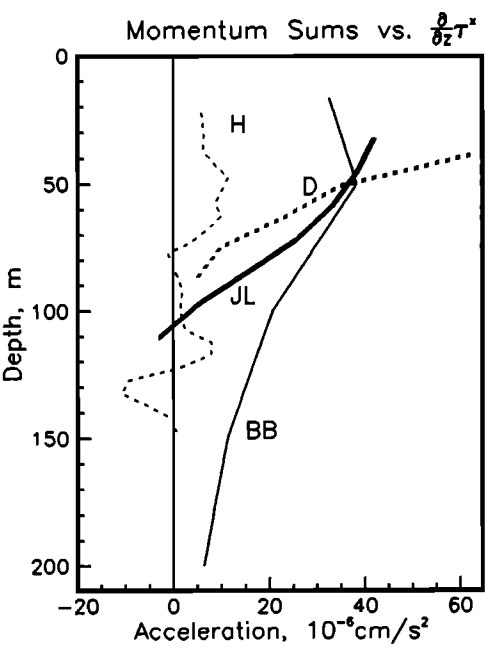

Figure 17. A comparison of the annual-averaged zonal momentum residual on the equator (dark, solid curve; data taken from Figure 15, middle) with *Bryden and Brady*'s [1989] result (light, solid curve). Above 80-m depth the two compare reasonably well but below that, Bryden and Brady have large residuals extending below the thermocline. The vertical structure of our estimate compares favorably with shorter timescale, dissipation-derived estimates of turbulent stress divergence from *Dillon et al.* [1989] (dark, dashed curve) and *Hebert et al.* [1991] (light, dashed curve). Stress data are courtesy of D. Hebert.

confined to the top 100 m of the ocean. Only forces deeper in the ocean can contribute to the discrepancy between the two studies; these are the pressure gradient, the mean advective forces, and the Coriolis force. Since the last is zero on the equator, where Bryden and Brady reported their results, only the first two need to be examined.

The zonal pressure gradients are very similar in the two studies, and meridional advection is small on the equator due to the approximate symmetry in the velocity fields. The major difference is found in zonal advection; *Bryden and Brady* [1985, 1989] find large eastward tendencies of 10–15 $\times$ 10^{-6} cm/s^2 due to zonal advection between 100-m and 170-m depth, consistent with the shoaling of the EUC eastward through their study region. In contrast, we find only smaller forces, less deeply distributed (e.g., Figure 10, top). It is possible that this difference between the studies is real, that the EUC shoaled less quickly between 158°W and 150°W than it did to the east during the Shuttle Experiment period. Model results, however, indicate that at these longitudes the EUC should be an inertial current below the thermocline [e.g., *Wacongne*, 1990] and thus that the zonal advective forces should be balanced by corresponding vertical advective forces. More probably, Bryden and Brady's larger zonal advective forces result from their use of geostrophy to estimate zonal currents near the equator. For example, their geostrophic currents at 150°W [*Bryden and Brady*, 1985, Figure 8a] have peak E*JC velocities over 30 cm/s faster than our concurrent, direct measurements between 150°W and 158°W. This biases their zonal advective forces positive, or eastward, by on the order of 10 $\times$ 10^{-6} cm/s^2 at that point. Since they restrict themselves to sections along 150°W, their time sampling scheme is also sparser than ours, leading to greater errors due to the large, geophysical variability.

Independent estimates of the vertical structure of turbulent, vertical stress can be derived from measurements of small scale dissipation and mean flow shear. *Dillon et al.* [1989] found strong vertical stresses on the equator at 140°W during a period of very strong winds. Their vertical stress divergence is superimposed on Figure 17 (dark, dashed curve). Because of the much smaller vertical scale of their stresses relative to *Bryden and Brady*'s [1985, 1989] momentum residual and because of the smallness of their shallowest stress estimate relative to their observed surface wind stress, Dillon et al. postulated that some unknown process besides vertical turbulent stress was transporting westward wind momentum downward into the ocean (see also *Wijesekera and Dillon* [1991]). Note, however, that the vertical scale of their stress profile is quite comparable to our annual-averaged, zonal momentum residual. *Hebert et al.* [1991] gathered similar dissipation measurements during a period of weak winds and found correspondingly weak stresses which, nonetheless, decayed quickly with depths to near zero at around 80 m. Again, this vertical structure is quite comparable to our momentum residual.

We conclude that the imbalance in *Bryden and Brady*'s [1985, 1989] momentum budget below the thermocline is probably erroneous, since our more directly measured estimate of the zonal momentum budget has a vertical structure in good agreement with the available, dissipation-derived estimates of turbulent vertical stresses. This finding argues against a need for more exotic processes transporting westward wind momentum downward. It does not, however, rule out such a possibility; *Dillon et al.*'s [1989] finding of shallow, vertical stresses which were insufficient to balance the observed surface wind stress still argues for some such process, at least during periods of high winds.

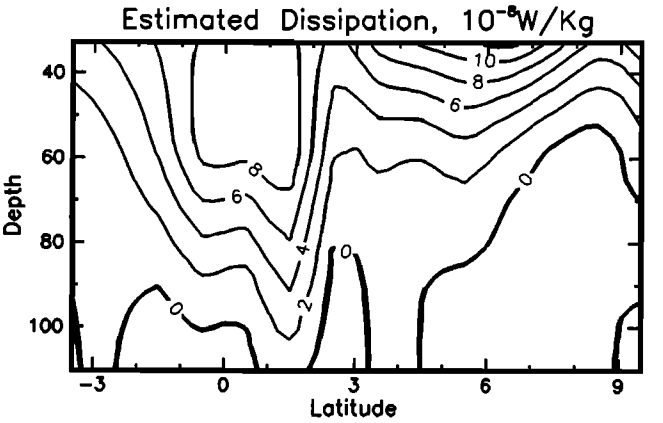

Figure 18. The estimated dissipation ε, given annual-averaged stresses which balance the momentum residual of Figure 15 (middle) and the annual-averaged vertical shears from Figure 3. The stronger, deeper dissipation on the equator is due not to larger, deeper stresses but to stronger mean flow shears.

6.4. Meridional Structure: Dissipation

Our second important result is the uniform depth of our momentum balance across the observed latitude band. This is in contrast to simple model results [e.g., *Stommel*, 1960] which imply that wind stresses, confined to a shallow Ekman layer in midlatitudes, should penetrate more deeply into the ocean as the equator is approached and the Coriolis parameter goes to zero. In apparent support of this expectation, the small scale, turbulent dissipation engendered by such vertical stresses has been observed to be strongest on the equator and also to penetrate more deeply there [*Peters et al.*, 1989; *Hebert et al.*, 1991; *Carr et al.*, 1992]. While producing a definitive model goes beyond the scope of this paper, we can at least reconcile our results to the observations of increased dissipation near the equator. *Peters et al.* [1989] emphasize that dissipation, being equal to turbulent kinetic energy (TKE) production, is substantially increased on the equator by the presence of mean flow shear. In fact, TKE production is a product of turbulent stress and vertical velocity shear [*Dillon et al.*, 1989]; thus the meridional and vertical structure of dissipation depends on the mean shear as well as on the vertical stresses. Presumably, the momentum residual of Figure 15 (middle) is equal to the negative of the vertical stress divergence; thus we form an estimate of annual-averaged vertical stress by integrating the momentum residual vertically from 117 m to any given depth. Multiplying these stresses by the mean flow shear gives us an estimate of annual-averaged dissipation due to mean flow shear.

This estimate (Figure 18) shows a significant increase in expected dissipation within a few degrees of the equator, much as observed in the studies cited above. It is apparent that this meridional dependence is due to the increased vertical shear of the EUC rather than to increased vertical stresses. Similarly, large values of dissipation occur deeper near the equator not because the stresses penetrate deeper

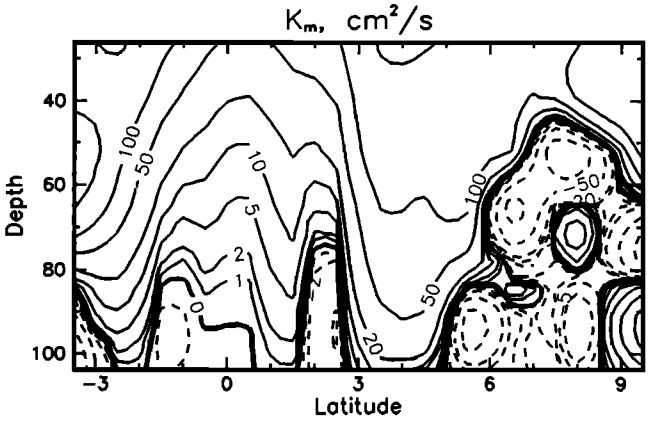

Figure 19. The coefficient of vertical eddy viscosity K_m, given annual-averaged stresses and vertical shears as for Figure 18. Note that above-thermocline viscosities are smaller on the equator than they are several degrees to the north or south.

there but because the strong, mean flow shear extends deeper. We find therefore that our observed momentum residual is entirely consistent with prior observations of dissipation.

6.5. Coefficient of Vertical Viscosity

If we define a coefficient of eddy viscosity,

$$K_m \frac{\partial \langle U \rangle}{\partial z} = \langle U^* W^* \rangle$$

and assume as in section 6.4 that the annual-averaged stresses are balanced by the annual averaged momentum residual, we can form an estimate for the annual-averaged eddy viscosity by dividing the derived stresses by the mean flow shear. This result is shown in Figure 19. On the equator the values range from around 1 cm^2/s near the EUC core to about 50 cm^2/s near the surface. *Wilson and Leetmaa* [1988] found very similar results in a comparable calculation using ADCP velocities along an equatorial section between 140°W and 100°W. Dissipation-derived estimates of vertical viscosity on the equator also yield very similar values [*Dillon et al.*, 1989; *Peters et al.*, 1988]. The agreement among all these studies is quite remarkable, given the wide range of time intervals used to define the mean quantities.

Off the equator our viscosity coefficients increase to values of 50–150 cm^2/s, commensurate with vertical stresses which are relatively uniform with latitude (Figure 15, middle) but mean flow shears which decrease rapidly beyond the bounds of the EUC. Negative values occur when the sign changes in mean shear and vertical stress do not exactly coincide. Though the negative viscosities can be quite large in magnitude due to the smallness of the mean shears, the stresses themselves are also generally small in these areas and so are probably not significant. The most we can conclude is that above the thermocline, where stresses are strong, the calculated viscosity is an order of magnitude stronger off the equator than on it.

Models incorporating vertical eddy viscosity often use a viscosity coefficient inversely proportional to the Richardson number to some power [*Pacanowski and Philander*, 1981]. While evidently adequate on the equator (e.g., *Wilson and Leetmaa* [1988], though *Peters et al.* [1988] fine-tune the power law at very low Richardson numbers), a Richardson number parameterization is clearly inadequate to describe the meridional variability of the present data. Above the thermocline the mean gradient Richardson number increases away from the equator since the squared, mean vertical shear (in the denominator of the Richardson number) weakens poleward faster than does the squared, mean stratification (in the numerator). The Pacanowski and Philander parameterization then implies that viscosity should decrease away from the equator, whereas our results show a strong increase.

It is known that transient, internal wave shears engender turbulent fluxes even where mean flow shears are weak. Insofar as the viscosity calculation above, or any other similar calculation, incorporates only the longtime mean shear, it may yield a different estimate of vertical eddy viscosity K_m than that appropriate for short-period turbulent stresses. It should also be noted, however, that viscosity may be less a function of mean flow shear than equatorial dissipation measurements alone have implied. Figure 20 shows the viscosity values within 3.5° of the equator, plotted as a function of mean flow shear and Väisälä frequency. The viscosities depend strongly on Väisälä frequency but do not increase with increasing shear as expected by turbulence theory; if anything, the reverse appears to be true. Note, too, that the annual-averaged bulk Richardson numbers are relatively large for the larger, off-equatorial viscosities. These results contradict not only the current Richardson number parameterizations but also the results of various turbulence closure schemes in numerical models [e.g., *Smith and Hess*, 1993]. While any attempt to parameterize vertical eddy viscosity in terms of bulk, long-term flow characteristics is doubtful at best (especially in the depth range of the diurnally cycling mixed layer (H. Peters, personal commu-

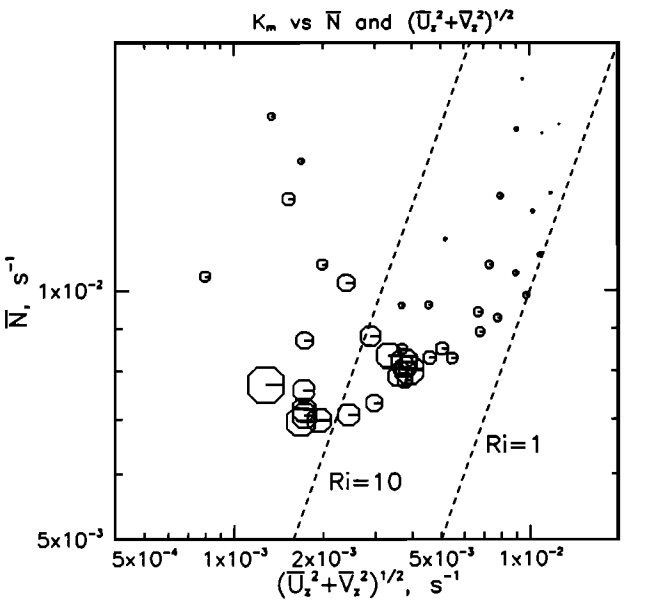

Figure 20. The viscosity values of Figure 19 scatterplotted as a function of mean shear and mean Väisälä frequency. Only positive values within 3.5° of the equator are shown. The magnitude of each viscosity value is proportionate to the area of the octagon marking its location; the largest value is about 350 cm/s^2.

nication, 1993)), our results indicate that *Pacanowski and Philander*'s [1981] Richardson number based scheme is clearly an inadequate test of the usefulness of such parameterizations.

6.6. Eliassen-Palm Fluxes

The extent to which the "eddies" interact with a background mean flow cannot be determined from measurements of eddy momentum fluxes alone; eddy heat fluxes also act to modify both the mean flow and the eddies themselves. *Eliassen and Palm* [1960] first addressed the issue of how these separate effects might cancel (see *Weisberg and Weingartner* [1988] for a cogent description of the subsequent development of the technique and its derivation). Briefly, the mean heat equation is assumed to be in steady state, with the effects of eddy heat fluxes exactly balanced by a mean vertical/meridional circulation which is regarded as being induced by the eddies. The effects of this induced circulation in the mean momentum equation can then be balanced against the direct effects of eddy momentum fluxes; if the two cancel, then the mean momentum equation is also in steady state, and the eddies are shown to have no net interaction with the mean flow.

Carrying through the Eliassen-Palm formalism here results in no such cancellation. Though the effects of the "induced" circulation are comparable in magnitude to the direct eddy momentum fluxes, they generally add to those fluxes rather than canceling them. Thus we conclude that the eddies during the Shuttle Experiment period did interact strongly with the mean flow. *Bryden and Brady* [1989] drew a similar conclusion from their momentum analysis. Further, any eddy-induced mean circulation is already included in our observed mean circulation. Thus any attempt to attribute part of the observed circulation to the eddies under an Eliassen-Palm formalism amounts to a bookkeeping exercise, relevant perhaps in determining the exact effect of the eddies on the mean flow but ultimately having no effect on the mean momentum balance itself. Since there are difficulties in applying the formalism here (notably its assumptions of vertically uniform stratification and mean zonal invariance, both flagrantly violated in the upper equatorial oceans), we will not provide a more formal determination of the effects of the eddies.

6.7. Is the Wind-Forced Divergence Centered on the Equator?

In section 4.1 we noted that the surface divergence of mean meridional velocity was not centered on the equator but rather near 2°N. Simple Ekman dynamics would imply that since wind stress is relatively uniform with latitude and the Coriolis parameter changes sign at the equator, the meridional wind drift should exhibit a strong divergence centered roughly on the equator. *Poulain* [1993] has confirmed this expectation with a long-term average of drifter velocities near the equator between 90°W and 150°W. The overwhelming majority of his data, however, is from east of 130°W; his results in the 150°–160°W longitude band are inconclusive due to sparsity of data.

While the errors of our observed mean meridional velocity are substantial (4 cm/s rms), it is unlikely that the true, near-surface divergence was centered on the equator during the Shuttle Experiment. Our observational errors are roughly invariant with depth (see section 3.3) and so should affect the surface divergence and the subsurface convergence equally. Hence an assumption of errors sufficient to move the observed surface divergence onto the equator would also move the subsurface convergence off the equator, an equally counterintuitive result. Thus we are forced to accept the mean meridional velocity field as observed, subject to reasonable uncertainties. It is possible that the presence of the Line Islands has perturbed the mean flow slightly, as part of this island chain lies within the study region.

7. Summary and Conclusions

We have used a year of ADCP and CTD data from the NORPAX Hawaii-to-Tahiti Shuttle Experiment to explore the mean zonal momentum balance in the tropical mid-Pacific. We decomposed 27 cross-equatorial sections using a multiple linear regression into mean, annual cycle, and higher-frequency flow fields. The mean field explicitly includes an east-west trend, which was observed with good statistical confidence in both zonal velocity and pressure. We then determined the effects of the various flow fields on the mean momentum balance. All relevant forces were determined except vertical stresses, most with acceptable statistical confidence.

Our major finding is that even neglecting vertical stresses, the zonal momentum equation is in rough balance at 90–117-m depths at all latitudes from 4°S to 10°N. Presumably, this balance holds at deeper levels as well, although these were not observed by the ADCP employed and the PCM data were too noisy to make this determination. The formal error bars on our calculation are large, but the fact that our observed balance at 90-m depth is reproducible over four or five statistically independent latitudes indicates that it is real. Of the terms contributing to this balance at 90-m depth, the largest is the eastward pressure gradient which is strong within 4° of the equator. At and poleward of 3°, this pressure gradient is opposed by the Coriolis forces of the mean meridional convergence in a geostrophic balance. Nearer the equator, the Coriolis forces combine with advective forces from the mean meridional convergence to balance the pressure gradient to within 1° of the equator, while meridional eddy stresses balance the residual eastward forces on the equator itself. Smaller contributions are made by other mean and eddy advective terms.

Nearer the surface, the zonal momentum equation is dominated by the eastward forces of the pressure gradient (near the equator) and the eastward Coriolis forces of a strong, northward Ekman flow (north of 2°N). In the vertical integral these forces roughly balance the surface wind stress. It is of interest that the northward Ekman flow appears to penetrate into the shoaling thermocline north of the NECC.

The implication of our momentum balance is that the vertical stresses arising from wind forcing need not penetrate deeper than 90 m into the tropical ocean at any latitude. This contradicts an earlier study of the equatorial zonal momentum budget by *Bryden and Brady* [1985, 1989], but it is consistent with the penetrations implied by turbulent dissipation measurements on the equator. Similarly, previous findings of stronger, deeper dissipation profiles on the equator than off the equator are probably due to the stronger, deeper mean shears prevailing there rather than to latitude dependent stress profiles. Finally, annual-averaged vertical

turbulent viscosities derived from our observations agree with previous estimates on the equator but increase in value both to the north and to the south. This poleward increase in viscosity occurs despite increasing Richardson numbers, in clear contradiction of current Richardson number based parameterizations of turbulent viscosity.

Appendix: Error Calculations

The disagreement between our large error estimates and the latitudinal uniformity of the momentum balance in Figure 15 provoked us to look more closely at our error estimates. Our initial parametric error estimates (as in LJ) assumed that the various terms on the right-hand side of the zonal momentum equation (2) were statistically independent and therefore that their error variances added to give the error variance of the total. In fact, the terms sum at any instant to equal the local acceleration, which is not necessarily large. In such a case the variability of the momentum sum (i.e., the local acceleration) might be smaller than the variability of its component terms, and thus error bars based on the assumption of statistical independence would be too large. The solution is to estimate the errors of the sum as a whole. While this sum is a large and complicated expression, its errors can be easily estimated using the bootstrap method.

The bootstrap technique [*Efron*, 1979] utilizes computational rather than analytic resources. In brief, the samples available for analysis are viewed as a set of stochastic samples whose statistics are representative of the real world. The variance of a statistic of N real world samples is found by simply selecting N samples at random from the representative set and calculating that statistic, repeating this process many times until a stable value for the statistic's variance emerges. This is identified as the mean square error of the statistic. The advantages of the method are two; firstly, the calculation of errors is no harder than that of the statistic itself, only more computer intensive; and secondly, no assumptions need to be made about the probability distribution of the data.

We implemented this method by randomly sampling from the 27 cross-equatorial sections to form 500 sets of 27 sections each. On each set we performed the MLR and zonal momentum analysis as detailed in section 3, retaining the variance of all the results across the 500 sets. The error estimates which emerged were actually larger than the parametric estimates; these are compared on the equator in Figure 21. The fault in our analysis was this; we assumed that the 27 sections were identically prepared realizations of a random process. In fact, the sections occurred at differing parts of the annual cycle and so were not random. Subsampling the 27 sections resulted in data sets which were (in general) oversampled in some parts of the annual cycle and undersampled in others. This destroyed the orthogonality between the various components of the MLR, resulting in large estimated errors in those fields. The solution to this problem is to remove the mean and annual cycle fields first, performing the bootstrap process on the residual, high-frequency variance. This reduces the degrees of freedom available by 6, biasing the residual variance to smaller values; in a parametric analysis this is countered by increasing the errors associated with the residual variance by a factor of $N/(N - 6)$. We do the same here with our bootstrap estimates of the errors of (2) and add in a parametric estimate of the errors due to the (previously removed) annual cycle term. The resulting combined errors match our original parametric errors closely (Figure 21).

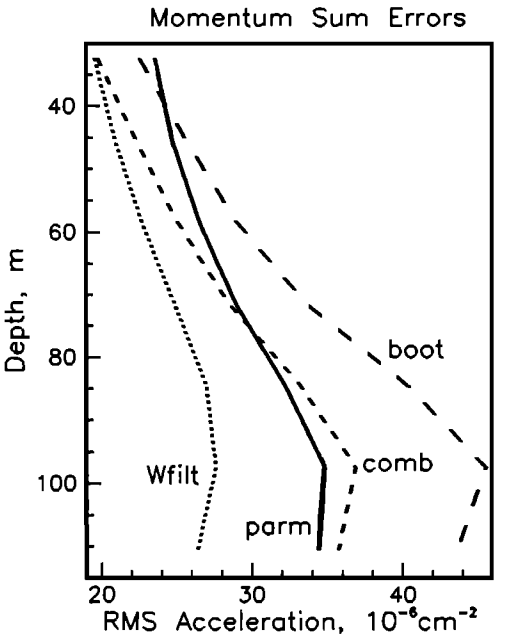

Figure 21. A comparison of error estimates on the equator. The initial bootstrap estimate (boot) is larger than parametric estimates (parm); but a more careful, parametric treatment of the annual cycle resulted in a combined bootstrap estimate (comb) which agreed well with the parametric result. Filtering mean vertical velocity over 3° latitude reduced navigation noise on the equator, producing the final, combined estimate (Wfilt).

The close match between the parametric and combined bootstrap error estimates implies that the parametric assumption of independence between the major terms of (2) is, in fact, valid. We confirm this by summing the bootstrap error variances for the individual terms using the assumption of independence; the result closely matches the bootstrap errors calculated for the sum as a whole (not shown).

The large errors near the equator are exacerbated by uncertainties in mean vertical velocity. Since we know from Figures 3 and 5 that the scales of horizontal convergence are several degrees of latitude (but see *Poulain* [1993]), we can average mean vertical velocity over 3° of latitude with little loss of structure. This results in greatly reduced errors near the equator, mostly by reducing navigational noise in the horizontal velocities. Our final error estimates incorporate this averaging of mean vertical velocity into the above combination of bootstrap errors with parametric treatment of the annual cycle.

While of interest to statisticians, the above exercise failed to identify any assumption in our calculation of errors which would result in unrealistically large estimates.

Acknowledgments. The extensive efforts of L. Regier, R. Knox, and D. Cutchin in deploying and shepherding the ADCP during the Shuttle Experiment are gratefully acknowledged, as are the hours spent by G. Anderson in editing raw data tapes. The PCM data were kindly provided by E. Firing, as were the dissipation-derived quantities by D. Hebert. This work was supported by NSF grants OCE88-17706 (E.S.J. and D.S.L.) and OCE90-12851 (D.S.L.) to the

Scripps Institution of Oceanography, University of California at San Diego, and by OCE-9202737 (E.S.J.) to the Joint Institute for the Study of the Atmosphere and Oceans, University of Washington. Contribution 240 from the Joint Institute for the Study of Atmosphere and Oceans and contribution 1505 from the Pacific Marine Environmental Laboratory, NOAA.

References

Bryden, H. L., and E. C. Brady, Diagnostic model of the three-dimensional circulation in the upper equatorial Pacific, *J. Phys. Oceanogr.*, *15*, 1255–1273, 1985.

Bryden, H. L., and E. C. Brady, Eddy momentum and heat fluxes and their effects on the circulation of the equatorial Pacific Ocean, *J. Mar. Res.*, *47*, 55–79, 1989.

Carr, M-E., N. S. Oakey, B. Jones, and M. R. Lewis, Hydrographic patterns and vertical mixing in the equatorial Pacific along 150°W, *J. Geophys. Res.*, *97*, 611–626, 1992.

Dillon, T. M., J. N. Moum, T. K. Chereskin, and D. R. Caldwell, Zonal momentum balance at the equator, *J. Phys. Oceanogr.*, *19*, 561–570, 1989.

Efron, B., Computers and the theory of statistics: Thinking the unthinkable, *SIAM Rev.*, *21*, 460–480, 1979.

Eliassen, A., and E. Palm, On the transfer of energy in stationary mountain waves, *Geophys. Norv.*, *22*, 1–23, 1960.

Firing, E., C. Fenander, and J. Miller, Profiling current meter measurements from the NORPAX Hawaii to Tahiti Shuttle Experiment, *Data Rep. 39, HI6-81-2*, 146 pp., Hawaii Inst. of Geophys., Univ. of Hawaii, Honolulu, 1981.

Halpern, D., R. A. Knox, and D. S. Luther, Observations of 20-day period meridional current oscillations in the upper ocean along the Pacific equator, *J. Phys. Oceanogr.*, *18*, 1514–1534, 1988.

Hebert, D., J. N. Moum, C. A. Paulson, D. R. Caldwell, T. K. Chereskin, and M. J. McPhaden, The role of the turbulent stress divergence in the equatorial Pacific zonal momentum balance, *J. Geophys. Res.*, *96*, 7127–7136, 1991.

Johnson, E. S., Studies of Doppler acoustic velocities measured during the NORPAX Hawaii-to-Tahiti Shuttle, Ph.D. dissertation, Scripps Inst. of Oceanogr., La Jolla, Calif., 1987.

Johnson, E. S., and M. J. McPhaden, Effects of a three-dimensional mean flow on intraseasonal Kelvin waves in the equatorial Pacific Ocean, *J. Geophys. Res.*, *98*, 10,185–10,194, 1993.

Johnson, E. S., L. A. Regier, and R. A. Knox, A study of geostrophy in tropical Pacific Ocean currents during the NORPAX Tahiti Shuttle using a shipboard Doppler acoustic current profiler, *J. Phys. Oceanogr.*, *18*, 708–723, 1988.

Kendall, T. R., *The Pacific Equatorial Countercurrent*, 79 pp., International Center for Environmental Research, Laguna Beach, Calif., 1970.

Knauss, J. A., Further measurements and observations on the Cromwell Current, *J. Mar. Res.*, *24*, 205–240, 1966.

Lukas, R., and E. Firing, The geostrophic balance of the Pacific Equatorial Undercurrent, *Deep Sea Res., Part A*, *31*, 61–66, 1984.

Luther, D. S., and E. S. Johnson, Eddy energetics in the upper equatorial Pacific during the Hawaii-to-Tahiti Shuttle Experiment, *J. Phys. Oceanogr.*, *20*, 913–944, 1990.

Mangum, L. J., and S. P. Hayes, The vertical structure of the zonal pressure gradient in the eastern equatorial Pacific, *J. Geophys. Res.*, *89*, 10,441–10,449, 1984.

McPhaden, M. J., and B. A. Taft, Dynamics of seasonal and intraseasonal variability in the eastern equatorial Pacific, *J. Phys. Oceanogr.*, *18*, 1713–1732, 1988.

Meyers, G., Annual variation in the slope of the 14°C isotherm along the equator in the Pacific Ocean, *J. Phys. Oceanogr.*, *9*, 885–891, 1979.

Moum, J. N., M. J. McPhaden, D. Hebert, H. Peters, C. A. Paulson, and D. R. Caldwell, Internal waves, dynamic instabilities, and turbulence in the equatorial thermocline: An introduction to three papers in this issue, *J. Phys. Oceanogr.*, *22*, 1357–1359, 1992.

Pacanowski, R. C., and S. G. H. Philander, Parameterization of vertical mixing in numerical models of tropical oceans, *J. Phys. Oceanogr.*, *11*, 1443–1451, 1981.

Peters, H., M. C. Gregg, and J. M. Toole, On the parameterization of equatorial turbulence, *J. Geophys. Res.*, *93*, 1199–1218, 1988.

Peters, H., M. C. Gregg, and J. M. Toole, Meridional variability of turbulence through the equatorial undercurrent, *J. Geophys. Res.*, *94*, 18,003–18,009, 1989.

Philander, S. G. H., W. J. Hurlin, and A. D. Seigel, Simulation of the seasonal cycle of the tropical Pacific Ocean, *J. Phys. Oceanogr.*, *17*, 1986–2002, 1987.

Poulain, P., Estimates of horizontal divergence and vertical velocity in the equatorial Pacific, *J. Phys. Oceanogr.*, *23*, 601–607, 1993.

Sadler, J. C., B. Kilonsky, M. A. Hori, M. A. Lander, and L. K. Oda, Surface winds, wind stress, and weather over the tropical Pacific during the FGGE Hawaii to Tahiti oceanographic shuttle January 1979–June 1980, *Tech. Rep. UHMET 83-01*, 109 pp., Dep. of Meteorol., Univ. of Hawaii, Honolulu, 1983.

Smith, N. R., and G. D. Hess, A comparison of vertical eddy mixing parameterizations for equatorial ocean models, *J. Phys. Oceanogr.*, *23*, 1823–1830, 1993.

Stevenson, J. W., Computation of heat and momentum fluxes at the sea surface during the Hawaii-to-Tahiti Shuttle Experiment, *Rep. HIG-82-4*, 42 pp., Hawaii Inst. of Geophys., Univ. of Hawaii, Honolulu, 1982.

Stommel, H., Wind-drift near the equator, *Deep Sea Res.*, *6*, 298–302, 1960.

Taft, B. A., and W. S. Kessler, Variations of zonal currents in the central tropical Pacific during 1970 to 1987: Sea level and dynamic height measurements, *J. Geophys. Res.*, *96*, 12,599–12,618, 1991.

Taft, B. A , B. M. Hickey, C. Wunsch, and D. J. Baker, Jr., Equatorial undercurrent and deeper flows in the central Pacific, *Deep Sea Res.*, *21*, 403–430, 1974.

Wacongne, S., Dynamical regimes of a fully nonlinear stratified model of the Atlantic equatorial undercurrent, *J. Geophys. Res.*, *94*, 4801–4815, 1989.

Wacongne, S., On the difference in strength between Atlantic and Pacific Undercurrents, *J. Phys. Oceanogr.*, *20*, 792–799, 1990.

Weisberg, R. H., and T. J. Weingartner, Instability waves in the equatorial Atlantic Ocean, *J. Phys. Oceanogr.*, *18*, 1641–1657, 1988.

Wijesekera, H. W., and T. M. Dillon, Internal waves and mixing in the upper equatorial Pacific Ocean, *J. Geophys. Res.*, *96*, 7115–7125, 1991.

Wilson, D., and A. Leetmaa, Acoustic Doppler current profiling in the equatorial Pacific in 1984, *J. Geophys. Res.*, *93*, 13,947–13,966, 1988.

Wyrtki, K., and B. Kilonsky, Mean water and current structure during the Hawaii-to-Tahiti Shuttle Experiment, *J. Phys. Oceanogr.*, *14*, 242–254, 1984.

E. S. Johnson, Pacific Marine Environmental Laboratory, NOAA, 7600 Sand Point Way NE, Seattle, WA 98115.

D. S. Luther, School of Ocean and Earth Science and Technology, University of Hawaii at Manoa, Honolulu, HI 96822.

(Received September 13, 1993; revised December 14, 1993; accepted December 16, 1993.)